EUROPEAN ORGANIZATION FOR NUCLEAR RESEARCH

CERN–EP/90–42
4 April 1990

AN EMULSION STUDY OF ^{16}O AND ^{32}S INTERACTIONS AT 200 GeV PER NUCLEON SELECTED BY TRANSVERSE ENERGY

The HELIOS–Emulsion Collaboration

T. Åkesson[4], S. Almehed[10], A.L.S. Angelis[8], S. Aoki[15], N. Armenise[2], H. Atherton[4], P. Aubry[12], G. Baroni[18], H.W. Bartels[7], G. Beaudoin[12], J.M. Beaulieu[12], H. Beker[4], O. Benary[22], D. Bettoni[4a], V. Bisi[24], I. Blevis[25], H. Bøggild[4b], A.C. Breslin[5], W. Cleland[17], M. Clemen[17], B. Collick[17], F. Corriveau[11], S. Dagan[22], D.H. Davis[8], K. Dederichs[4c], S. Dell'Uomo[18], P. Depommier[12], R.C.E. Devenish[4d], N. DiGiacomo[9], S. Di Liberto[18], J.R. Dodd[26], B. Dolgoshein[12], A. Drees[6], H. En'yo[4], B. Erlandsson[21], M.J. Esten[8], C.W. Fabjan[4], P. Fischer[7], Z. Fraenkel[25], A. Gaidot[19], F. Gibrat-Debu[19], P. Giubellino[24], P. Glassel[7], U. Goerlach[4], G. Grella[20], R. Haglund[10], L.A. Hamel[11], H. van Hecke[9], V. Hedberg[4], R. Heifetz[22], A. Holscher[7], K. Hoshino[15], T. Ishigami[23], B. Jacak[9], G. Jarlskog[10], S. Johansson[10], M. Kazuno[23], H. Kitamura[15], M. Kobayashi[15], Y. Kobayashi[23], K. Kodama[1], H. Kraner[3], V. Kroh[7], F. Lamarche[11], C. Leroy[11], D. Lissauer[3,22], G. London[19], B. Lorstad[10], A. Lounis[12], A. Marzari-Chiesa[24], M. Masera[24], M.A. Mazzoni[4], E. Mazzucato[11], M.L. McCubbin[8], P. McGaughey[9], F. Meddi[18], M. Miyanishi[15], U. Mjornmark[10], M.T. Muciaccia[2], S. Muraviev[13], M. Murray[17], K. Nakamura[15], S. Nakanishi[15], K. Nakazawa[6], M. Neubert[7], S. Nilsson[21], K. Niu[15], K. Niwa[15], M. Nomura[15], L. Olsen[3], Y. Oren[22], J.P. Pansart[19], Y.M. Park[17], A. Pfeiffer[7], F. Piuz[4], V. Polychronakos[3], G. Poulard[4], M. Price[4], D. Rahm[3], L. Ramello[24], L. Riccati[24], G. Romano[20], G. Rosa[18], L. Sandor[4], S. Sartori[24], J. Schukraft[4], M. Sekimoto[4e], B. Sellden[21], M. Seman[4f], C. Sgarbi[18], H. Shibuya[23], A. Shmeleva[13], V. Sidorov[16], S. Simone[2], Y. Sirois[11], H. Sletten[4], S. Smirnov[14], J. Soltani[7], W. Sondheim[9], H.J. Specht[7], I. Stumer[3], J. Sunier[9], H. Tajima[15], V. Tcherniatin[14], H.H. Thodberg[4], J. Thompson[17], V. Tikhomirov[13], D.N. Tovee[8], I. Tserruya[25], K. Tsukagoshi[15], Y. Umezawa[23], N. Ushida[1], G. Vasseur[19], R. Veenhof[4g], S. Watanabe[23], R. Wigmans[4] and P. Yepes[11]

(Submitted to Nuclear Physics B)

Footnotes on next page.

1) Aichi University of Education, Kariya, Japan.
2) University of Bari and INFN, Bari, Italy.
3) Brookhaven National Laboratory, Upton, NY, USA.
4) CERN, Geneva, Switzerland.
5) University College Dublin, Ireland.
6) Faculty of Education, Gifu University, Gifu, Japan.
7) University of Heidelberg, Fed. Rep. Germany.
8) University College London, UK.
9) Los Alamos National Laboratory, Los Alamos, N. Mex., USA.
10) University of Lund, Sweden.
11) McGill University, Montreal, Canada.
12) University of Montreal, Canada.
13) Lebedev Institute of Physics, Moscow, USSR.
14) Institute of Physics and Engineering, Moscow, USSR.
15) Department of Physics, Nagoya University, Nagoya, Japan.
16) Institute of Nuclear Physics, Novosibirsk, USSR.
17) University of Pittsburgh, Pa., USA.
18) University of Rome 'La Sapienza' and INFN, Rome, Italy.
19) DPhPE, CEN–Saclay, Gif-sur-Yvette, France.
20) University of Salerno and INFN, Salerno, Italy.
21) University of Stockholm, Sweden.
22) Tel Aviv University, Ramat Aviv, Israel.
23) Department of Physics, Toho University, Funabashi, Japan.
24) University of Turin and INFN, Turin, Italy.
25) Weizmann Institute of Science, Rehovot, Israel.

Visitor at CERN from:

a) University of Syracuse, NY, USA.
b) Niels Bohr Institute, Copenhagen, Denmark.
c) Ludwig-Maximilians-Universität, Munich, Fed. Rep. Germany.
d) Oxford University, Oxford, UK.
e) Institute of Nuclear Study, Tokyo, Japan.
f) Slovak Academy of Sciences, Kosice, Czechoslovakia.
g) NIKHEF-H, Amsterdam, The Netherlands.

ABSTRACT

Interactions of ^{16}O and ^{32}S at 200 GeV per nucleon in emulsion and in emulsion–tungsten chamber targets were tagged by transverse energy and multiplicity triggers in the HELIOS apparatus at CERN. As a first sample, 375 events, covering a wide range of transverse energies, were located and studied in emulsion. Results are reported in this paper. The angular distribution has been measured, event by event, with a wide pseudorapidity coverage, both in emulsion and in the HELIOS calorimeters. The total charged multiplicity and the transverse energy per charged particle have been obtained as a function of the transverse energy and of the pseudorapidity. The measured distributions are compared with the predictions of the Dual Parton Model, as coded in the IRIS generator. Assuming that 59% of the E_T is transported by charged particles, and estimating the energy density by a full transparency picture, a comparison with cosmic-ray data has also been attempted.

1. INTRODUCTION

Extended volumes of excited hadronic matter can be created in ultrarelativistic nucleus–nucleus collisions. It is believed that a phase transition to a plasma of deconfined quarks and gluons, the quark–gluon plasma (QGP), can occur [1], provided the energy density reaches some critical value. Recent lattice QCD calculations predict a critical temperature of $\sim$ 200 MeV, corresponding to an energy density of the order of 2.5 GeV/fm^3 [2]. The order at which the phase transition happens remains still in question, either 'weak' first order or second order [3].

Whether or not a phase transition occurred, either in extended thermalized volumes or in hot blobs, excited states ultimately decay into observable ordinary hadrons, and a large excitation energy should finally induce high particle multiplicity and large transverse-energy flow.

An important experimental programme on this subject is being pursued [4, 5]. The first aim is to survey the general properties of ultrarelativistic nucleus–nucleus collisions and to compare the data with model calculations based on extrapolations from p–p and p–nucleus data. Any deviation could signal the onset of new physics. The second aim is to explore specific probes of QGP, once the general features of the reaction dynamics are understood.

The global observables of main interest are the differential cross-section as a function of the multiplicity and of the transverse energy ($E_T = \sum E_i \sin\theta_i$), the rapidity density, and the inclusive p_T distributions. These observables, which can be studied for different target and beam nuclei, and at different energies, are linked to the energy density and to the entropy density of the interaction.

In this paper, measurements of some global parameters by a hybrid-emulsion technique are reported. In particular, the correlation between transverse energy, multiplicity, and rapidity density is investigated for ^{16}O–emulsion, ^{32}S–emulsion, and ^{32}S–W interactions at 200 GeV per nucleon in different pseudorapidity*) intervals.

Specific signals, such as charm production, rapidity-density fluctuations, two-particle and many-particle rapidity correlations, could probe [6] the excited states and the possible QGP more directly. They are studied on event samples collected during the same data taking: results on charmed particles have already been published [7]; other analyses are in progress.

2. EXPERIMENTAL PROCEDURE

2.1 Experimental set-up and data-taking

Nuclear emulsions were exposed to ^{16}O and ^{32}S beams at 200 GeV per nucleon in the target region of the HELIOS (High-Energy Lepton and IOn Spectrometer) detector at CERN [8, 9].

In the 'hybrid' set-up, sketched in fig. 1a, a beam hodoscope (BH), consisting of two doublets of silicon microstrip detectors, provided the coordinates of the interacting beam particles, transverse to the beam direction. The detectors were 2×2 cm^2 and 300 μm thick, with an analog multiplexed readout of the 50 μm pitch Si strips.

*) The pseudorapidity is defined as $\eta = -\ln\tan(\theta/2)$. For $p_T \gg m$, $\eta \sim y$ where y is the rapidity, so that a good approximation to rapidity is obtained from an angle measurement only.

The BH was placed in front of a movable emulsion stack holder, controlled by a microprocessor and equipped with a precise optical readout of the stage coordinates. This stage mover (SM) was synchronized with the beam spill and interfaced to the HELIOS data-acquisition system. This equipment was previously used in a similar configuration in the WA75 experiment [10].

The target stacks were composed of 16 × 25 cm^2 emulsion sheets, either double-coated or single-layer, held perpendicular to the beam direction, the most downstream sheets being interleaved with honeycomb spacers (fig. 1b). In some exposure configurations, thin target foils of tungsten were inserted between the upstream emulsion sheets. The stacks exposed to ^{32}S were sandwiched between thin CR-39 plastic track detector sheets. All the emulsion plates were freshly prepared at the CERN pouring facility [11] before the exposures, and processed soon afterwards.

The target thicknesses for pure emulsion and emulsion–tungsten exposures to ^{16}O and ^{32}S beams ranged from 5 to 10% of an interaction length.

Downstream from the emulsion, two silicon ring counters (RCs) were set up, followed by a silicon pad detector (SP) [12] during the ^{16}O exposure in 1986, and by a third RC during the ^{32}S exposure in 1987. The RCs were segmented silicon detectors, 300 μm thick and 60 mm in diameter, with ring-shaped pads of radially increasing pitch (270 to 1200 μm), arranged in 32 rings subdivided into 12 angular sectors [13]. They were conceived as devices of nearly constant granularity as a function of pseudorapidity. The SP consisted of an array of 400 segments of variable size.

The silicon/emulsion instrumentation was placed inside the wide-acceptance HELIOS calorimeter system [14]. The backward c.m. region was covered by U–Cu/scintillator and Fe/scintillator (calorimetrized dipole magnet) sampling calorimeters, having a 20 × 20 cm^2 tower structure. In the forward region, a low-granularity U/scintillator calorimeter, used in the 1986 data-taking with an ^{16}O beam [8], was replaced in 1987 by a highly segmented U/liquid-argon calorimeter [9, 15].

The pseudorapidity acceptances of the above-listed detectors are indicated in table 1. Since the emulsion target was displaced by 42.6 cm upstream of the standard NA34 target position, these values are slightly different from those quoted in refs. [8], [9], and [14].

During the data-taking, $\sim 5 \times 10^3$ particles per burst, from a beam with a FWHM of about 2 mm, were spread over the emulsion target in a pattern of vertical lines under control of the SM. A nearly uniform emulsion exposure density of 10–30 tracks per square millimetre was achieved. Before and after the irradiation of each stack, the SM was kept at rest in suitable positions during a few bursts in order to mark 'beam spots' for intercalibration purposes [11, 16].

The first-level trigger was defined as a valid beam signal from small scintillator counters, calibrated to tag the beam charge, and an interaction signal ($\gtrsim$ 10 hits) in the forward silicon counters. For the transverse-energy trigger, the weighted sum of calorimeter signals in $0.1 \leq \eta \leq 3.0$ was required to exceed an assigned threshold value [9]. In the data-taking with ^{32}S, the E_T trigger was put in 'OR' with an on-line multiplicity trigger in RC1+RC2 set at > 250 counts. Minimum-bias events were also collected with a down-scaling factor of 8, keeping the overall trigger rate down to $\sim$ 50 events per burst.

About 3.3 litres of emulsion were exposed to ^{16}O, with a total integrated flux of $\sim 2 \times 10^7$ beam particles, producing $\sim 1 \times 10^6$ interactions in the target and $\sim 1 \times 10^5$ triggered events recorded on tape. In the case of ^{32}S, about 2.3 litres of emulsion were exposed, with an integrated flux of 6×10^6 beam particles, producing $\sim 3 \times 10^5$

interactions and $\sim 5 \times 10^4$ events on tape.

2.2 Off-line analysis

The off-line analysis of the BH, SM, RCs, and calorimeter data allowed the selection of events which occurred in emulsion and for which the information was complete.

A single cluster of hits was required in each of the four planes of the BH in order to define the coordinates of the incoming beam particle and to reject upstream interactions producing multiple-cluster patterns. The SM event coordinates were required to be within a fiducial region, i.e. events near to the edges or close to the beam spots were rejected. In the case of oxygen, a severe reduction of the available event sample was due to inefficiencies in the BH readout chain.

The off-line hit pattern in the RCs (and SP) was obtained for each event by gain calibration for all the individual pad elements. Events with peculiar hit-pattern features or with abnormal hit multiplicities could then be selected for scanning.

The off-line analysis of the scintillator calorimeters' data followed the procedure described in ref. [8]. The energy calibration was based on cosmic muons and electron beam data. Corrections for the geometry of the backward calorimeter system were computed by Monte Carlo: the sharing of the shower-particle signals among many towers and the space-angle dependence of the absorber length were thus accounted for. The transverse energy in various pseudorapidity intervals was finally calculated, taking into account the position of the emulsion target.

The analysis of the forward U/Ar calorimeter for emulsion data is in progress. An extensive study of the correlation between energy flow and multiplicity over the full η-range covered is planned for the data collected with the ^{32}S beam. For the purposes of the present analysis, E_T is defined as the transverse energy summed over particles contained in the range $0.1 \leq \eta \leq 3.0$.

2.3 Emulsion analysis

After a suitable cut on E_T, the final sample of events was available for scanning. Events collected so far were mainly selected in the high-E_T region, whereas a number of events were sampled at lower E_T for reference.

To locate the selected events in emulsion, a precise intercalibration procedure was applied to each stack [10]. The centre of gravity of the beam spots, reconstructed in the BH reference frame, was also measured in the individual reference frame (grid) of the emulsion plates.

When this had been done, interactions were searched for within a cylinder of $\sim$ 300 μm diameter around the nominal transverse position of the interacting beam particle, determined by the SM and BH coordinates. Since the longitudinal position remained unknown, the scanning was performed over all the plates, but the interaction was clearly indicated by shower-particle tracks already in the most downstream plate, and the procedure was quick and efficient. In the case of double-coated sheets, using the technique of minimodules [11] and automatized microscope systems, the scan took only a few minutes per event.

Because of the low exposure density (for $\sim$ 20 beam particles per square millimetre, there is $\lesssim 1$ interaction), events were unambiguously identified, with a spread of $\lesssim$ 100 μm in the difference between measured and expected coordinates transverse to the beam. The hit pattern in RCs could also be compared with the track pattern in emulsion for further confirmation.

The high multiplicities of the events required computer-aided measuring devices. The microscope image was observed on a monitor through a high-resolution solid-state CCD camera.

The search for tracks due to secondary charged particles was intended to cover the full solid angle. In the case of the W–emulsion chambers, whenever events that occurred in W were studied, particles emitted at angles wider than a cut value ($\theta > 45°$–$90°$, depending on the longitudinal vertex position) were not detected. Tracks were classified as 'black' (no gap, continuous track), 'grey' (grain clusters with some gap) and 'shower' (light tracks, due to close-to-minimum-ionizing particles), with no attempt to measure the ionization. Projectile fragments of charge 2 or more surviving the interaction, would have been detected if present: none was found in our sample.

The transverse position of the interaction vertex was defined by the beam particle, measured upstream of the interaction point. The vertex position along the beam was measured directly for events that occurred in emulsion, whereas in the case of events that occurred in the W target, a fit over several grain coordinates was performed for a few inclined secondary tracks.

The track angles were determined by single-point measurements. Nearby tracks of non-interacting beam particles were used both as a reference and to correct for distortion. The single-grain coordinates were measured by combining the light-spot coordinates on the TV screen with the coordinates of the microscope stage read by optical rulers. The stage was driven to subsequent fields by step or DC motors under the control of the host computer. Graphic characters were superimposed on the measured points, so that an easy check of the measurements was possible. In this way a fairly complete angular coverage was achieved, at the same time avoiding double measurements of tracks. The complete measurement of each event required a few hours.

A very high multiplicity ^{32}S–W event, as it appeared near the vertex, is shown in fig. 2c; in fig. 2e the same event is shown $\sim$ 1 mm downstream, whilst in figs. 2a and 2d the beam tracks are displayed as they are seen in the CR-39 sheets before and after the emulsion stack. The CR-39 plates are not sensitive to minimum-ionizing particles, so that in the downstream CR-39 plate, only the tracks of non-interacting beam particles are visible. Figure 2f presents the pseudorapidity distribution, as obtained with this procedure, for the event shown in figs. 2c and 2e.

The accuracy of the track-angle measurements given by this method is far from the best that one could obtain in emulsion by multigrain measurements and line-fit. Indeed, in order to check the detection efficiency, the systematic errors, and the accuracy, a few events were measured repeatedly by different operators. Comparing the results, most of the measured tracks were unambiguously matched, typically 95%. For low-multiplicity events, mismatches and lost tracks were found mostly at very wide angles. In high-multiplicity events they were concentrated at very forward angles, since in certain cases it was not possible—or not practical—to extend the track search far away from the vertex.

Systematic errors in track angles are due to the uncertainty in the transverse ($\sim 2\ \mu$m) and longitudinal ($\sim 5\ \mu$m) vertex coordinates, and to corrections for shrinkage, plate expansion, and distortion. In terms of pseudorapidity, absolute values of η are not fully reliable for $\eta > 6$. Statistical errors in single-track measurements are due to the uncertainty of the single-grain transverse ($< 2\ \mu$m) and longitudinal ($< 5\ \mu$m) coordinates. By comparing the values of the space angle or of the related pseudorapidity for matching tracks obtained in repeated measurements, the differences as shown in fig. 3 were found. The accuracy in space angle thus ranges from $< 0.2°$ at forward angles to

$\sim 1.0°$ at wide angles. In terms of pseudorapidity, a rather constant spread of ≤ 0.1 unit is obtained, up to $\eta \sim 4.5$; it then grows to > 0.5 for higher values.

In the following discussion, only shower particles are considered: pions with momentum $\lesssim$ 100 MeV/c and protons of momentum $\lesssim$ 600 MeV/c are thus excluded.

3. RESULTS

The results presented in this paper concern a first sample of 375 events selected off-line to study the ion interactions as a function of the transverse-energy flow in the calorimeters. The sample includes 110 O–emulsion events, 188 S–emulsion events, and 77 S–W events, at 200 GeV per nucleon.

3.1 Track multiplicity as a function of E_T

In order to clarify how the selection affects the results, some features of the differential E_T cross-section, $d\sigma/dE_T$, will be briefly recalled.

Systematic measurements of $d\sigma/dE_T$ were performed—among other experiments—by HELIOS [8, 9], with ^{16}O and ^{32}S beams accelerated at 200 GeV per nucleon (for ^{16}O also at 60 GeV per nucleon) on various target nuclei. However, as explained in the previous section, the η acceptance with thin passive targets was slightly different from that with the emulsion target. It turns out that a constant factor of ~ 0.95 has to be applied in order to rescale the HELIOS 'backward E_T' ($-0.1 \leq \eta \leq 2.9$) cross-section data to the emulsion set-up:

$$E_T \text{ (passive target, } -0.1 \leq \eta \leq 2.9) = 0.95 \times E_T \text{ (emulsion target, } 0.1 \leq \eta \leq 3.0).$$

The values plotted in fig. 4 have been obtained from the data of refs. [8] and [9] with such a rescaling. After a peak at low E_T due to peripheral processes, a decrease of the cross-section is observed down to a flat region, often referred to as the 'plateau', followed by a steep 'tail'. This well-known shape is determined essentially by the impact parameter: the shoulder point*) between plateau and tail corresponds to the full overlap of the projectile and target density distributions, i.e. to collisions with an impact parameter equal to the difference between the nuclear radii. A selection of events with E_T above the shoulder point corresponds to $\sim$ 3.7% of the total inelastic cross-section for ^{16}O–Ag, to $\sim$ 1.4% for ^{32}S–Ag, and to $\sim$ 1.8% for S–W. On the other hand, the transverse energy at the shoulder point, $E_T^{shoulder}$, has been seen to depend on the target mass as A_{target}^{α}, with $\alpha \approx 0.5$ [9]. Actual values can be found in refs. [8] and [9]. Thus, a high-E_T selection applied to interactions in emulsion effectively removes contributions from the light components (H, C, N, O, ...), whilst only 'central' interactions on Ag (Br) are kept. For reference in the following discussion, we quote $E_T^{shoulder} \approx 90$ GeV for ^{16}O–Ag, $E_T^{shoulder} \approx 165$ GeV for ^{32}S–Ag, and $E_T^{shoulder} \approx 210$ GeV for ^{32}S–W, on the E_T scale of the HELIOS-Emulsion set-up.

As shown in fig. 5, the total charged-particle multiplicity turns out to be strongly correlated with E_T over the observed E_T range. Different symbols are used to identify projectile and target. In the case of ^{32}S on W, where multiplicities as high as $\sim$ 650 were recorded, the limited acceptance in track detection at backward angles should be taken into account, with an estimated loss of $\leq$ 10%. Figures 6a to 6f show in more

*) $E_T^{shoulder}$ is defined [8] as the value of E_T for which the cross-section is 50% of the 'plateau' value.

detail, again as a function of E_T, that the increase in multiplicity is mostly observed in the intermediate rapidity region. In the rapidity bin $2.0 < \eta < 3.0$, data for different projectile–target systems do overlap. Target fragmentation effects appear in rapidity bins $1.0 < \eta < 2.0$, where W entries are higher than Ag (Br), and $3.0 < \eta < 4.0$, where W entries are lower. At very forward angles, a flattening and then a depletion is observed, with limiting values reminiscent of the identity of the projectile nucleus. These results could be useful in the comparison of inclusive data obtained with different η acceptances. At very small impact parameters, missing forward energy and 'forward E_T' signals tend to saturate, whereas the 'inelasticity' of the interactions is still increasing, mainly affecting the target and projectile rapidity regions.

Taking advantage of the granularity of the HELIOS calorimeters, the multiplicity and the E_T can be measured in the same angular region. As an example, single-event data are reported in fig. 7a, referring to the rapidity window $1.4 < \eta < 3.0$ and to the full range in the azimuthal angle. In such a broad interval, the measurements of the multiplicity and of E_T appear to be almost equivalent. Moreover, all the events seem to lie close to a common curve, irrespective of the nature of projectile and target nuclei, with no dramatic change in the slope of such an average curve in the explored domain. The quantity E_T per charged particle in the same η window has the distribution shown in fig. 7b, with a mean value of 678 MeV and a r.m.s. of 108 MeV.

3.2 Homogeneous subsamples. A comparison with IRIS.

In order to study multiplicity and E_T in narrow η bins, and to compare quantitative results with model-based calculations, homogeneous event subsamples must be considered, i.e. with the same projectile–target system and impact parameter of the collisions. For this reason, in table 2 we define the event subsamples listed below by E_T windows (again in $0.1 < \eta < 3.0$) and by the corresponding fraction of the total inelastic cross-section.

It should be noted that all these event subsamples, including 295 events out of 375, are representative of very inelastic ion collisions.

Figure 8a shows the rapidity-density distribution, averaged over events in the same class in the domain of such 'central' collisions. From shoulder to tail, the peak is shifted to lower values, whilst the distribution tends to shrink. Similar trends were observed by other experiments [17] and by the present experiment with an analysis of the silicon counters [18]. In the tail region, rapidity densities as high as 80, 135, and 180 charged particles per unit of rapidity are reached with the beams and targets quoted in table 2. Moreover, much higher values, by up to a factor of 2, are often attained for individual events (fig. 8b), as rapidity-density spikes. The statistical significance of such fluctuations is being investigated with appropriate techniques, and will not be discussed here.

Compared with other experiments using nuclear emulsions [19, 20], significantly higher multiplicities and rapidity densities are observed in our case, owing to the strict selection of central interactions by E_T. For instance, peak rapidity densities of ~ 110 are reported by the EMU01 Collaboration [20] for interactions with more than 300 minimum-ionizing particle tracks. Their subsample amounts to $\sim 3\%$ of all the S–emulsion interactions, and it is estimated to correspond to $\sim 5.3\%$ of the S–Ag(Br) total inelastic cross-section. This selection would correspond to a cut in our sample close to the 'plateau' region.

In a simplified geometrical picture, the ion collisions involve a number of 'participant' nucleons proportional to the volume of the overlap region. At zero impact

parameter, for ^{16}O and ^{32}S projectiles on heavier targets, all the projectile nucleons are expected to participate, as well as an effective number of target nucleons:

$$A_{eff} = (3/2)A_{proj}^{2/3} \cdot A_{target}^{1/3} \quad .$$

The pseudorapidity of the c.m. system η_{cm} is a function of the c.m. energy of the participant system

$$\eta_{cm} = \ln\left(\frac{s^{1/2}}{A_{eff} \cdot m}\right) \quad ,$$

where m is the nucleon mass and

$$s = \left(A_{proj}^2 + A_{eff}^2\right) m^2 + 2E_{beam} A_{eff} m \quad .$$

In our cases, at 200 GeV per nucleon,

	O–Ag	S–Ag	S–W
A_{eff}	45	72	86
η_{cm}	2.51	2.62	2.53

whereas if $A_{eff} \rightarrow A_{target}$, i.e. in the projectile–target c.m.s.,

A_{target}	108	108	184
η_{cm}	2.08	2.42	2.16

On the other hand, $\eta_{cm} = 3.03$ for nucleon–nucleon collisions at 200 GeV.

The distributions shown in fig. 8a for emulsion targets have a broad peak close to the η values expected for A_{eff} (Ag). However, in the case of W, a peak at $\eta(A_{eff} \rightarrow A_{target})$ shows up at the highest E_T. This result could signal significant reinteraction processes following a central collision on a large target, caused by the former 'spectators' producing hundreds of secondaries in the target fragmentation region.

One can attempt to compare the experimental data with the results of model-based calculations. As a first step, one should try to describe the ultrarelativistic nucleus–nucleus collisions by an incoherent superposition of constituent particle interactions. With this aim in view, events were generated by the recently updated IRIS code [21]. IRIS is a colour-exchange model based on Dual Parton (DP) concepts [22]. The parameters of the elementary parton–parton interactions are chosen according to e^+e^- and p–p data. Diffractive and hard processes are taken into account in addition to the soft DP processes. The excited parton states are hadronized according to the Lund Monte Carlo. The final state is built up after the decay of hadronic resonances. The aim of this approach is to describe p–nucleus and nucleus–nucleus data in a conservative framework, i.e. assuming no new physics input, such as collective behaviour or phase transition.

Monte Carlo generators available at present generally reproduce well the gross features of the data, reflecting mainly the geometry of the interactions. We do not intend to give here a detailed comparison of the various models, such as FRITIOF, VENUS, etc., whose predictions can be found elsewhere [23, 24]. The choice of IRIS is just to give an example of such predictions.

Events were generated by the IRIS code, obtaining differential E_T cross-section curves of the same shape as those observed in fig. 4. In order to apply the same impact parameter selection, IRIS event subclasses were defined, corresponding to the same fraction of the total inelastic cross-section. The generated rapidity-density curves

are superimposed on the experimental curves for corresponding event classes in fig. 8a, without normalization factors.

Whilst both the shape and the multiplicity content of the generated distributions are in fair agreement with those of the experimental distributions, discrepancies are observed, mainly in the target fragmentation region. Cascading effects, not accounted for in the model, could partly explain this disagreement.

For a more quantitative check, some relevant parameters are reported in table 3, where the number of events, the mean E_T, and the mean multiplicity are quoted for each event class. The increase in $\langle E_T \rangle$ is higher in the experimental data than obtained with IRIS, whilst the latter shows a higher increase for $\langle N_{ch} \rangle$. The rapidity density at peak, the mean value $\langle \eta \rangle$, and the r.m.s. $\sigma(\eta)$ are also reported, as well as the fraction of particles in pseudorapidity regions dominated by the target ($\eta < 1.0$) and projectile ($\eta > 5.0$) fragmentation. Note that $\langle \eta \rangle$ is systematically higher in IRIS, even if it tends to decrease from plateau to tail, as observed experimentally.

The main result from IRIS is that the transverse energy is proportional to the number of participating nucleons, whilst any memory of the original projectile–target system is lost. However, to obtain the same number of participants, and thus the same E_T, collisions having different impact parameters must be considered for different projectile–target systems. On the other hand, collisions having the same centrality must be compared in order to obtain A-dependences of the final-state parameters.

With this aim in view, the following ratios were calculated using the IRIS-generated data at peak rapidity density,

$$\frac{(dN/d\eta)_{\mathrm{S-Ag}}}{(dN/d\eta)_{\mathrm{O-Ag}}} = 1.83 \qquad \text{and} \qquad \frac{(dN/d\eta)_{\mathrm{S-W}}}{(dN/d\eta)_{\mathrm{S-Ag}}} = 1.17$$

for the event classes of shoulder and tail together, to be compared with the observed values of 1.60 for ^{32}S and ^{16}O on emulsion, and 1.31 for ^{32}S on emulsion and W. Thus the model seems to overestimate the dependence on A_{proj} and underestimate the dependence on A_{target}.

The quantity E_T per charged particle has been estimated as a function of η. Average values from events in the above-defined subclasses are reported in fig. 9, with IRIS results superimposed. This ratio tends to be higher than the value expected from IRIS. Moreover it appears to be slightly dependent on η: it seems to increase at lower η. However, note that the baryon content is certainly higher in the target fragmentation region than outside it, and this content may vary as a function of the impact parameter. We plan to investigate this trend by using higher statistics and full η calorimetry.

3.3 Trends in $\langle p_T \rangle$. Comparison with cosmic-ray data.

Finally, an attempt has been made to use the whole available event sample, irrespective of the subclasses previously defined, to study the dependence of $\langle p_T \rangle$ on some estimated value of the energy density ε reached in the collision. The $\langle p_T \rangle$ can be estimated by converting the measured value of E_T/charged particle to $\langle E_T \rangle$, with a constant factor of 0.59 estimated by the Lund fragmentation scheme. The systematic error on $\langle p_T \rangle$ is dominated by a systematic uncertainty in the absolute E_T scale, evaluated to be $\leq 10\%$.

In order to compare our data with cosmic-ray data, the definition of ε and of the interaction volume V used by the JACEE Collaboration [25] is applied; that is

$$\varepsilon = (3/2)(dN/d\eta)/V\sqrt{\langle p_T \rangle^2 + m_\pi^2}$$

$$V = \pi A_{proj}^{2/3} 2\tau_0 \quad ,$$

with the assumption $\tau_0 = 1$ fm/c *). The E_T and the charged-particle multiplicity were computed for each event in one unit of rapidity around the peak of the measured η distribution (i.e. close to the η region of the participating nucleons). The computed values are shown in fig. 10, where the JACEE results [25] with nuclei are also reported.

Compared with the JACEE results, we obtain substantially lower $\langle p_T \rangle$ values, with higher statistics and using a different experimental method, i.e. $\langle p_T \rangle \simeq 0.30$ GeV/c and $\simeq 0.40$ GeV/c, at $\varepsilon = 0.3$ GeV/fm^3 and 1 GeV/fm^3, respectively, instead of $\langle p_T \rangle \simeq 0.50$ GeV/c and $\simeq 0.60$ GeV/c.

Although the ε scale should be regarded as arbitrary, provided the same variables are used, it is noted that: a) the initial rise to a rather flat region reported by JACEE is observed, b) no further dramatic rise after the flat region is observed, although it seems that our events cover a region of ε values lower than the one accessed by cosmic-ray experiments.

4. CONCLUSIONS

Global parameters were measured in ^{16}O and ^{32}S 'central' interactions at 200 GeV per nucleon on Ag (Br) and W target nuclei, selected by the transverse energy E_T. Very high peak rapidity densities were observed, on the average, in the tail of the differential E_T cross-section, and even higher local values show up for individual events.

The predictions of a superposition model such as IRIS are in fair agreement with the data, but differences are found mainly in the target fragmentation region. The model tends to underestimate the dependence on the atomic number of the target and the attainable E_T values, whereas the dependence on the atomic number of the projectile, as well as the charged-particle multiplicity, are somewhat overestimated.

The rapidity distribution of the ratio E_T/N_{ch} has been measured in a limited pseudorapidity interval (backward in the c.m. frame) for events of different centrality. It is found to be constant as a function of the transverse energy in restricted rapidity bins, even in the tail of the differential cross-section. However, the distribution of E_T/N_{ch} is not flat in the region considered, and its shape depends on the projectile–target system and on the centrality of the interaction.

A comparison of our data with cosmic-ray data has been attempted, with respect to the correlation between the estimated values of average transverse momentum and energy density.

Acknowledgements

The authors wish to thank the CERN SPS Division for successful extraction of ion beams in 1986 and 1987, and the CERN EP Division for making available the pouring and processing facilities, with the necessary technical support.

The Emulsion Groups are very grateful to their scanning teams for their skilful measuring of such unusually high multiplicity events.

*) The definition of V differs slightly from that used in ref. [8], where $V = \pi R^2 \tau_0$, with $R = 1.14 A_{proj}^{1/3}$ fm and again $\tau_0 = 1$ fm/c.

REFERENCES

[1] E.V. Shuryak, The QCD vacuum, hadrons and the superdense matter (World Scientific, Singapore, 1988).

[2] F. Karsch, Z. Phys. **C38** (1988) 147.

[3] P. Bacilieri et al. (APE Collab.), Phys. Rev. Lett. **14** (1988) 1545 and Nucl. Phys. **B318** (1989) 553.
N. Christ et al., Phys. Rev. Lett. **14** (1988) 2050.
For a recent discussion, see the contributions of M. Fukugita, F.R. Brown and G. Parisi to the 1989 Symposium on Lattice Field Theory, Capri, 1989.

[4] Proc. Quark Matter '87, Nordkirchen, Z. Phys. **C38** (1988).

[5] Proc. Quark Matter '88, Lenox (Mass.), Nucl. Phys. **A498** (1989).

[6] K. Kajantie and L. McLarren, Annu. Rev. Nucl. Sci. **37** (1987) 293.
R.C. Hwa, Oregon Univ. preprint OITS 385 (1988).
A. Białas and R. Peschanski, Nucl. Phys. **B273** (1986) 703.

[7] S. Aoki et al., Phys. Lett. **B224** (1989) 441.

[8] T. Åkesson et al. (HELIOS Collab.), Z. Phys. **C38** (1988) 383.

[9] T. Åkesson et al. (HELIOS Collab.), Phys. Lett. **B214** (1988) 295.

[10] S. Aoki et al. (WA75 Collab.), Nucl. Instrum. Methods **A274** (1989) 64.
R. Alberganti et al., Nucl. Instrum. Methods **A248** (1986) 337.

[11] K. Hoshino and G. Rosa, Nucl. Track Rad. Meas. **12** (1986) 477.

[12] R. Beuttenmuller et al., Nucl. Instrum. Methods **A252** (1986) 471.

[13] P. Giubellino et al., Nucl. Instrum. Methods **A275** (1989) 89.

[14] T. Åkesson et al., Nucl. Instrum. Methods **A262** (1987) 243.

[15] T. Åkesson et al. (HELIOS Collab.), The measurement of the transverse energy flow in nucleus–nucleus collisions at 200 GeV per nucleon, in preparation.

[16] G. Romano, report CERN 85–18 (1985).

[17] A. Bamberger et al., Phys. Lett. **B184** (1987) 271 and **B205** (1988) 583.
R. Albrecht et al., Phys. Lett. **B202** (1988) 596.

[18] T. Åkesson et al. (HELIOS Collab.), preprint CERN–EP/89–97 (1989), to be published in Nucl. Phys. B.
M. Masera, Proc. 24th Rencontres de Moriond, Les Arcs, 1989, ed. J. Tran Thanh Van (Editions Frontières, Gif-sur-Yvette, 1989), p. 477.

[19] M.I. Adamovich et al., Phys. Lett. **B201** (1988) 397.
G. Singh et al., Phys. Rev. Lett. **61** (1988) 1073.
P.L. Jain et al., Phys. Rev. Lett. **59** (1987) 2531.
H. von Gersdorff et al., Phys. Rev. **C39** (1989) 1385.

[20] M.I. Adamovich et al., Phys. Lett. **B227** (1989) 285.

[21] J.P. Pansart, IRIS 306, Saclay report DPhPE 89–04 (1989).

[22] A. Capella and J. Tran Thanh Van, Phys. Lett. **93B** (1980) 146, and Nucl. Phys. **A461** (1987) 501c and references therein.

[23] B. Nilsson-Almqvist, Comput. Phys. Commun. **43** (1987) 387.
F. Lamarche, Ph.D. Thesis, McGill University (1989).

[24] K. Werner, Phys. Lett. **B208** (1988) 520.

[25] T.H. Burnett et al. (JACEE Collab.), Nucl. Phys. **A461** (1987) 263c.

Table 1
Pseudorapidity acceptances

	1986 run, ^{16}O		1987 run, ^{32}S	
	Detector	η	Detector	η
Silicon counter	RC1	1.0–3.0	RC1	1.0–3.0
	RC2	3.0–5.1	RC2	2.8–5.0
	SP	4.2–6.7	RC3	3.8–6.0
Backward calorimeters	U–Cu	0.1–2.3	U–Cu	0.1–2.3
	Fe	2.3–3.0	Fe	2.3–3.0
Forward calorimeters	U–Cu	> 3.0	ULAC	3.0–5.6

Table 2
Characteristics of event subsamples

	O–Ag (Br)		S–Ag (Br)		S–W	
	E_T (GeV)	Fraction of σ_{tot}^{inel} (%)	E_T (GeV)	Fraction of σ_{tot}^{inel} (%)	E_T (GeV)	Fraction of σ_{tot}^{inel} (%)
Plateau	45–75	12	110–150	5	150–195	5
Shoulder	75–105	6	150–180	2	195–225	2
Tail	> 105	< 2	> 180	< 1	> 225	< 1

Table 3
Comparison between measured quantities and IRIS predictions

	No. of events	$\langle E_T \rangle$	$\langle N_{ch} \rangle$	$dN/d\eta_{max}$	$\langle \eta \rangle$	$\sigma(\eta)$	Fraction of particles in $\eta > 5.0$ (%)	Fraction of particles in $\eta < 1.0^{*)}$ (%)
^{16}O–Ag (Br)								
Exp. data								
Plateau	35	57.2	165.8	48.6	2.95	1.52	9.1	9.5
Shoulder	25	89.5	222.0	66.8	2.86	1.42	7.0	8.6
Tail	27	117.7	261.9	78.5	2.80	1.35	5.6	8.4
IRIS								
Plateau	254	55.2	194.9	51.2	3.02	1.49	9.4	8.4
Shoulder	859	76.2	254.9	69.3	2.92	1.45	8.1	8.7
tail	296	94.3	294.9	82.9	2.84	1.42	6.8	9.2
^{32}S–Ag (Br)								
Exp. data								
Plateau	75	129.6	341.9	93.7	3.01	1.45	9.0	7.8
Shoulder	54	164.8	388.3	109.8	2.98	1.38	7.7	6.9
Tail	21	188.2	427.4	135.2	2.86	1.36	5.6	8.1
IRIS								
Plateau	95	112.1	410.2	116.3	3.10	1.44	9.5	6.5
Shoulder	44	133.9	466.8	130.2	3.03	1.42	8.7	7.1
tail	18	155.6	522.8	147.8	2.98	1.41	8.1	7.1
^{32}S–W								
Exp. data								
Plateau	29	173.0	429.6	132.1	2.83	1.29	< 5.4	> 6.8
Shoulder	15	204.9	477.5	150.7	2.82	1.29	< 5.7	> 7.0
Tail	14	248.7	546.6	177.9	2.74	1.25	< 4.4	> 7.1
IRIS								
Plateau	235	149.6	507.3	141.7	2.97	1.43	7.9	8.1
Shoulder	97	172.9	562.5	160.6	2.91	1.42	7.3	8.4
tail	53	192.0	600.5	175.4	2.86	1.41	6.9	8.7

*) Limited acceptance in pseudorapidity for W target: $\eta \geq 0.5$.

Figure captions

Fig. 1: a) Schematic layout of the set-up for emulsion exposures. b) Structure of the emulsion stacks and of the emulsion/W chambers.

Fig. 2: A central S–W interaction. a) Beam tracks in the first CR-39 plate. b) The same beam particles as seen in emulsion. c) The secondary tracks in emulsion close to the interaction vertex. d) The beam tracks in the CR-39 plate after the emulsions: only the non-interacting beam tracks are present. e) The secondary tracks 1 mm downstream from the interaction vertex. f) Pseudorapidity distribution.

Fig. 3: Differences in space angle (a) and in pseudorapidity (b) for matched tracks from independent event measurements.

Fig. 4: Differential cross-section $d\sigma/dE_T$ as a function of E_T ($-0.1 \leq \eta \leq 2.9$), from refs. [8] and [9] rescaled as explained in section 3.1.

Fig. 5: Total charged-particle (N_{ch}) multiplicity as a function of the 'centrality' selection parameter E_T ($0.1 \leq \eta \leq 3.0$).

Fig. 6: Charged-particle multiplicity (N_{ch}) in different η bins as a function of E_T ($0.1 \leq \eta \leq 3.0$).

Fig. 7: a) Charged-particle multiplicity (N_{ch}) as a function of E_T, both measured in the same η interval ($1.4 \leq \eta \leq 3.0$). b) E_T per charged particle in the same η window.

Fig. 8: a) Rapidity-density distributions ($\rho = N_{ev}^{-1}\ dN/d\eta$) in plateau, shoulder, and tail regions measured in emulsion for ^{16}O–emulsion, ^{32}S–emulsion and ^{32}S–W interactions. The dots represent the IRIS-generated distributions. b) Rapidity-density distributions for selected individual events in the tail region.

Fig. 9: Transverse energy per charged particle as a function of η from ^{16}O–emulsion, ^{32}S–emulsion, and ^{32}S–W events in plateau, shoulder, and tail regions: measured values (continuous line) and IRIS computation (dots).

Fig. 10: Distribution of $\langle p_T \rangle$ values versus energy density; ϵ is computed as in ref. [25]. Results from ref. [25] are also shown.

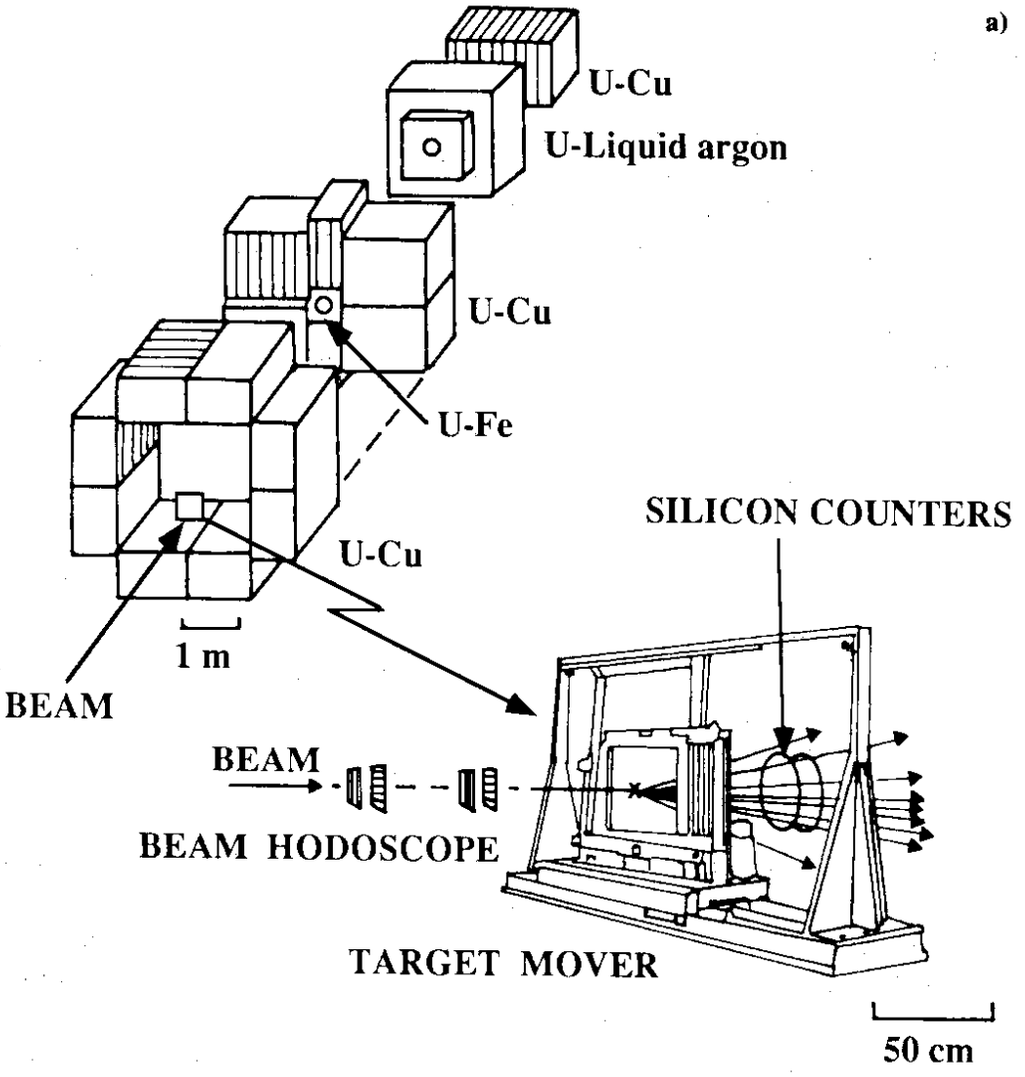
a)
U-Cu
U-Liquid argon
U-Cu
U-Fe
U-Cu
1 m
BEAM
SILICON COUNTERS
BEAM
BEAM HODOSCOPE
TARGET MOVER
50 cm

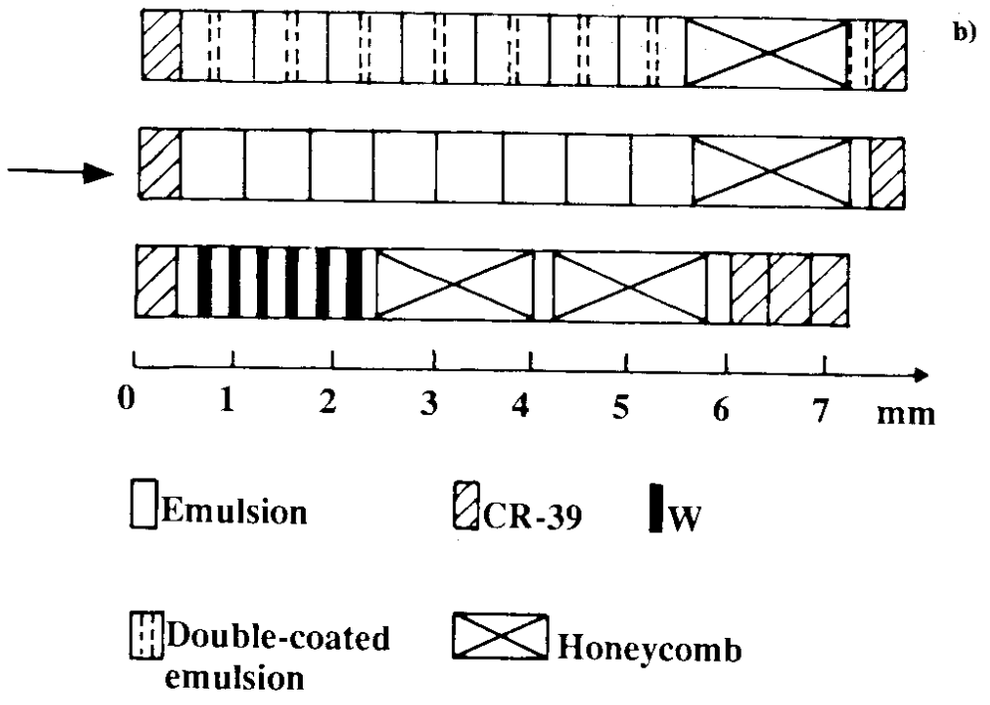
b)
0
1
2
3
4
5
6
7
mm
Emulsion
CR-39
W
Double-coated emulsion
Honeycomb

Fig. 1

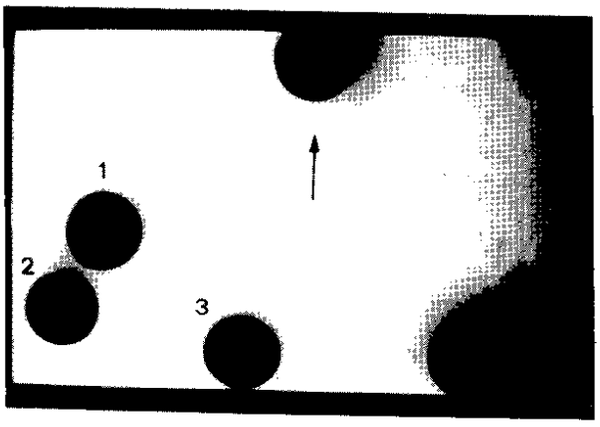
1
2
3

a)


1
2
3

b)


1
2
3

c)

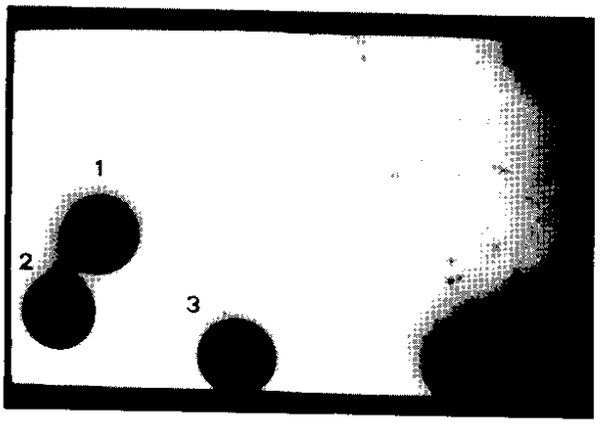
1
2
3

d)


NA34

e)

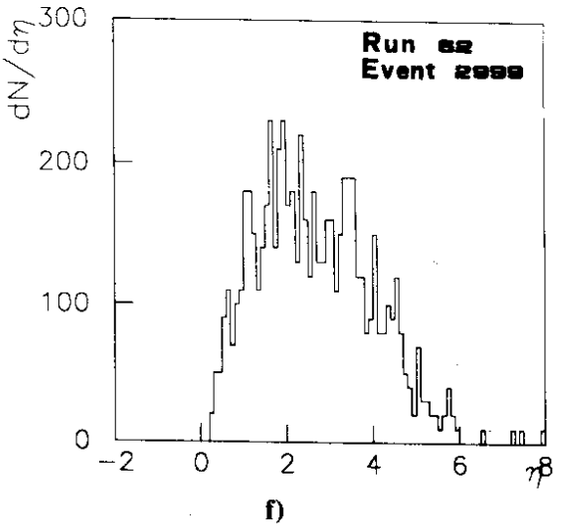
dN/dη
300
200
100
0
−2
0
2
4
6
η
Run 62
Event 2999

f)

Fig. 2

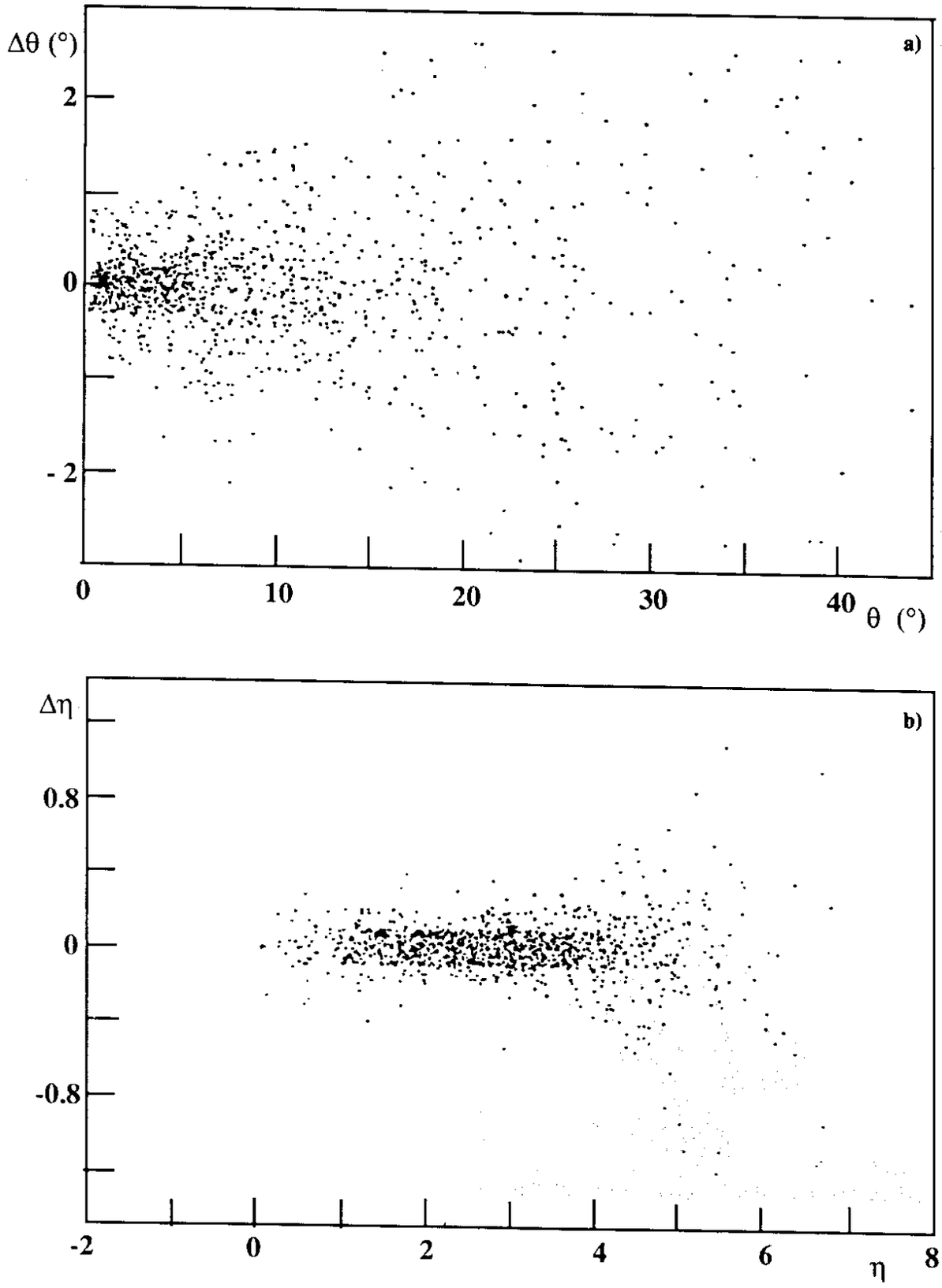

Fig. 3

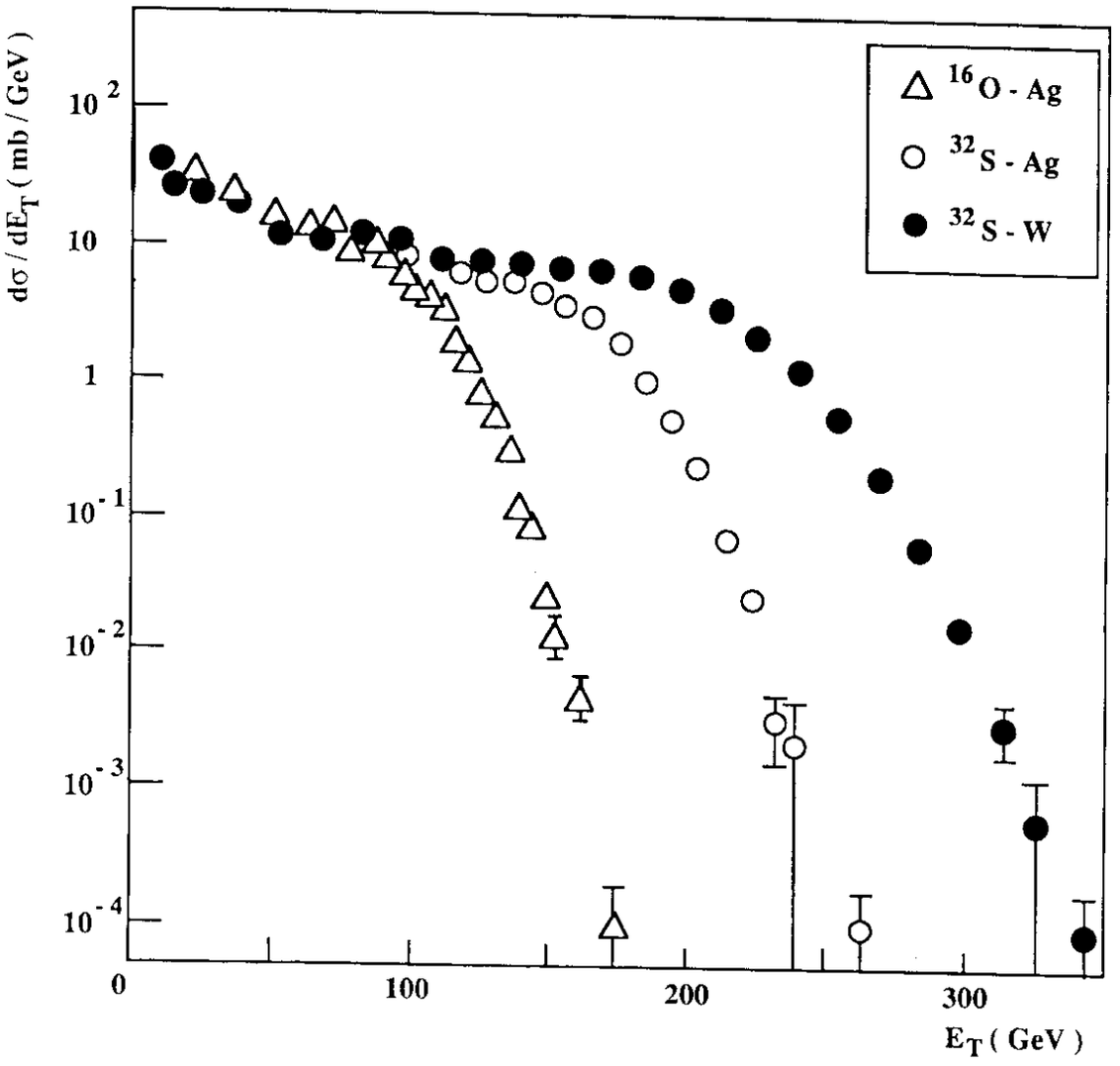
$d\sigma / dE_T$ (mb / GeV)
10^2
10
1
10^{-1}
10^{-2}
10^{-3}
10^{-4}
0
100
200
300
E_T (GeV)
^{16}O - Ag
^{32}S - Ag
^{32}S - W

Fig. 4

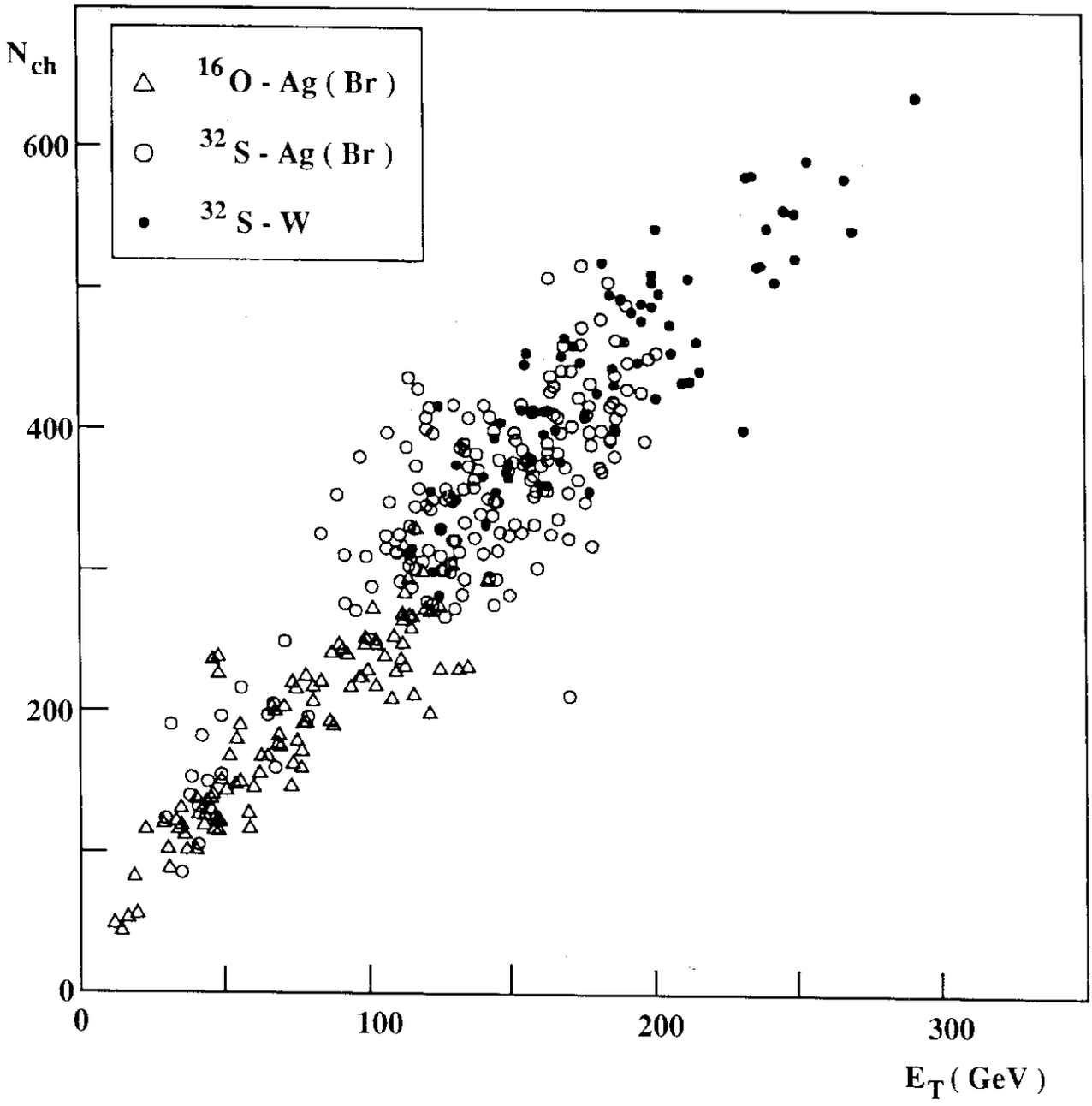

Fig. 5

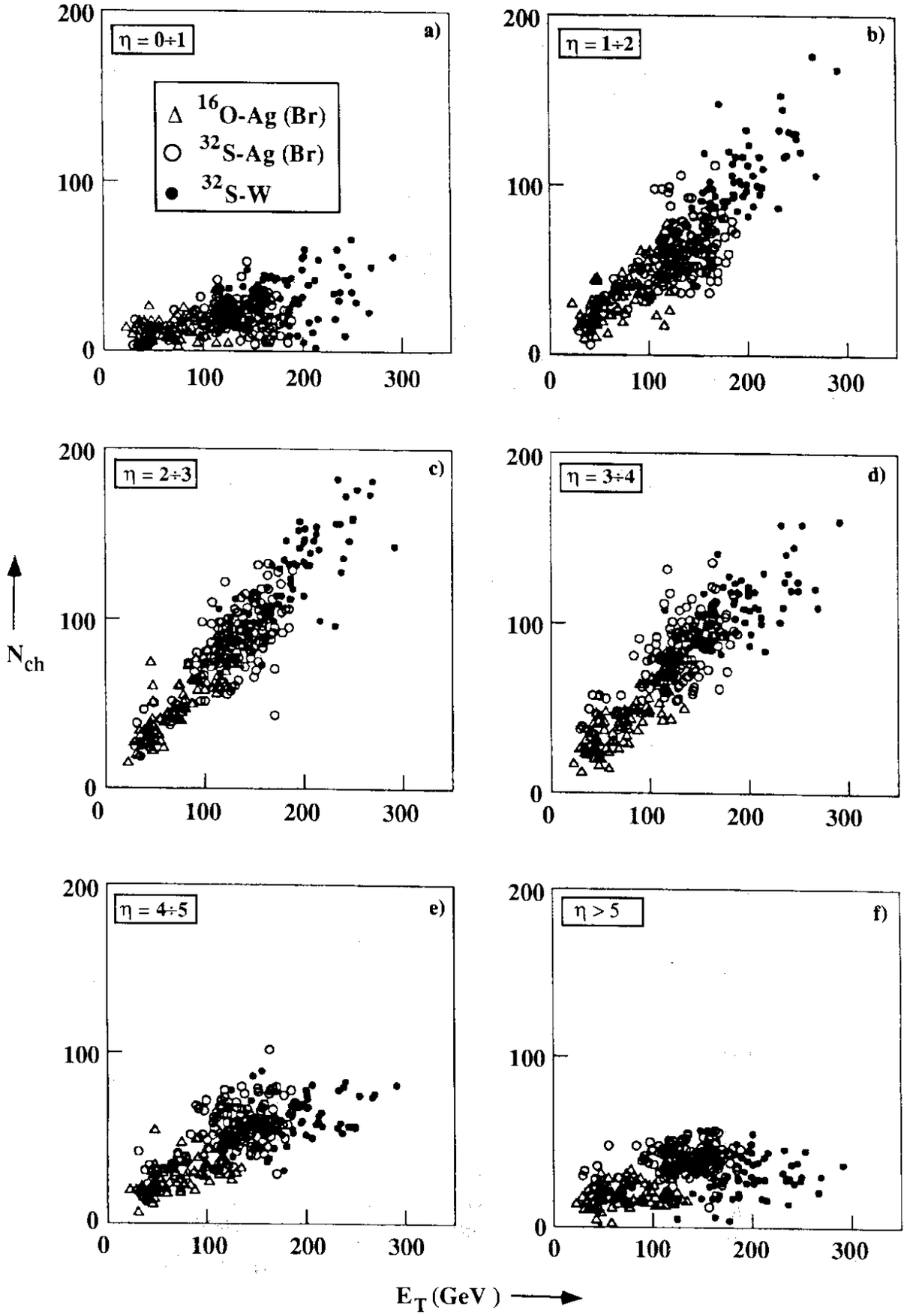
η = 0÷1
a)
Δ ^{16}O-Ag (Br)
○ ^{32}S-Ag (Br)
● ^{32}S-W
η = 1÷2
b)
η = 2÷3
c)
η = 3÷4
d)
η = 4÷5
e)
η > 5
f)
200
100
0
0
100
200
300
N_{ch}
E_T (GeV)

Fig. 6

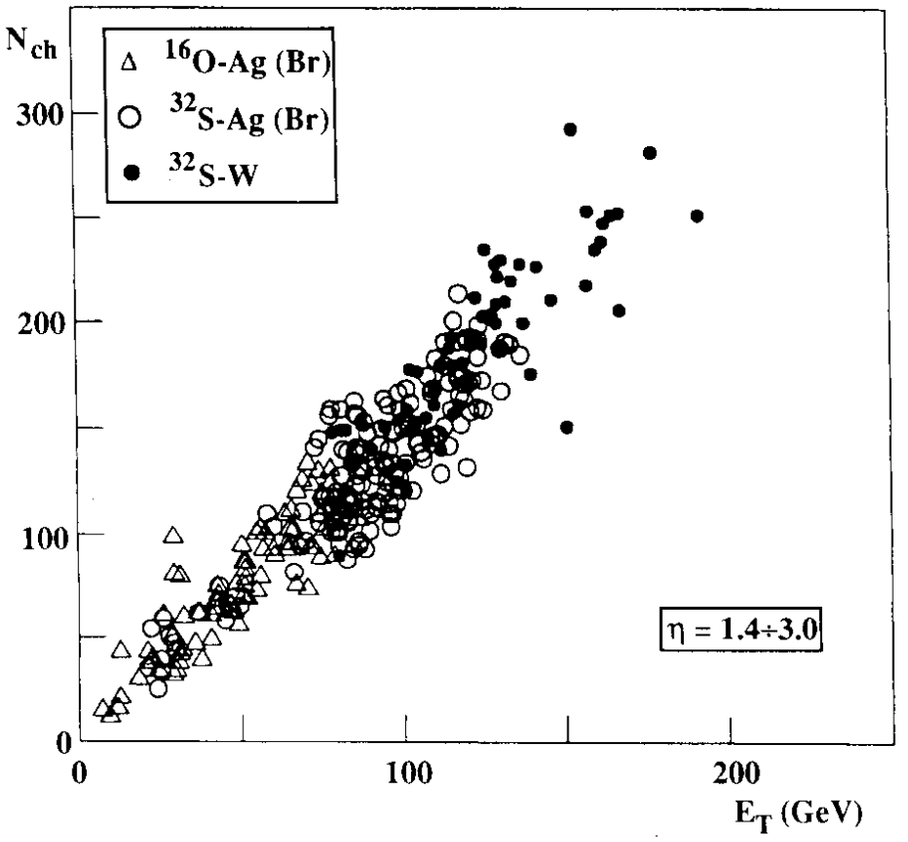
N_{ch}
^{16}O-Ag (Br)
^{32}S-Ag (Br)
^{32}S-W
300
200
100
0
0
100
200
E_T (GeV)
η = 1.4÷3.0

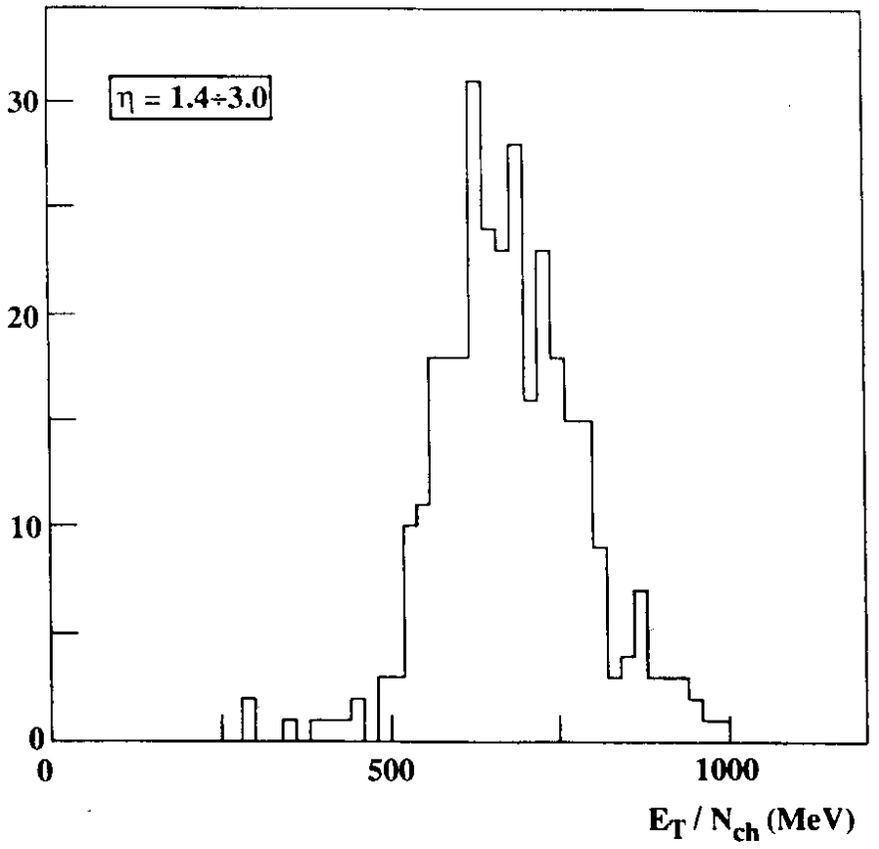
η = 1.4÷3.0
30
20
10
0
0
500
1000
E_T / N_{ch} (MeV)

Fig. 7

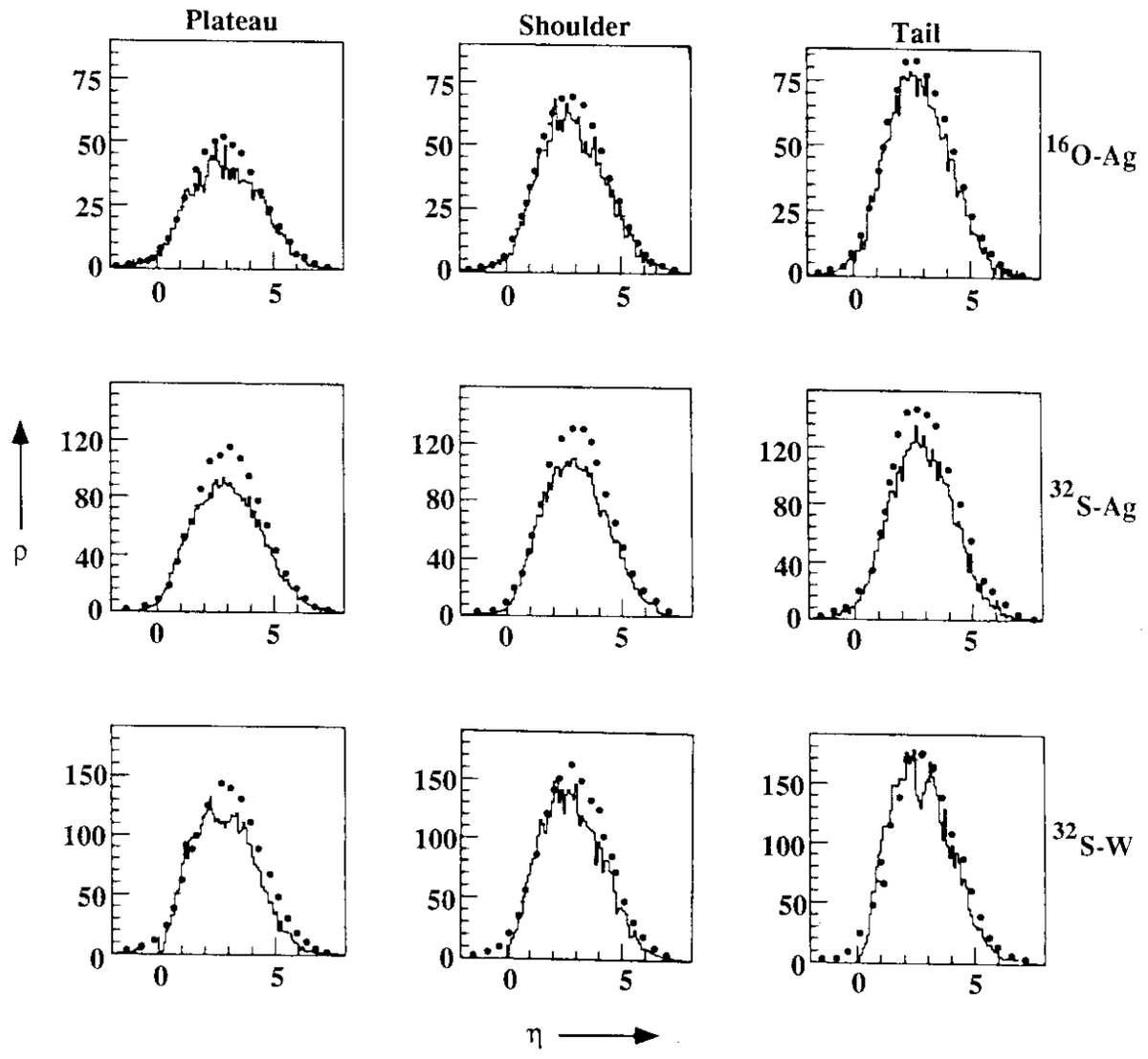

Fig. 8a

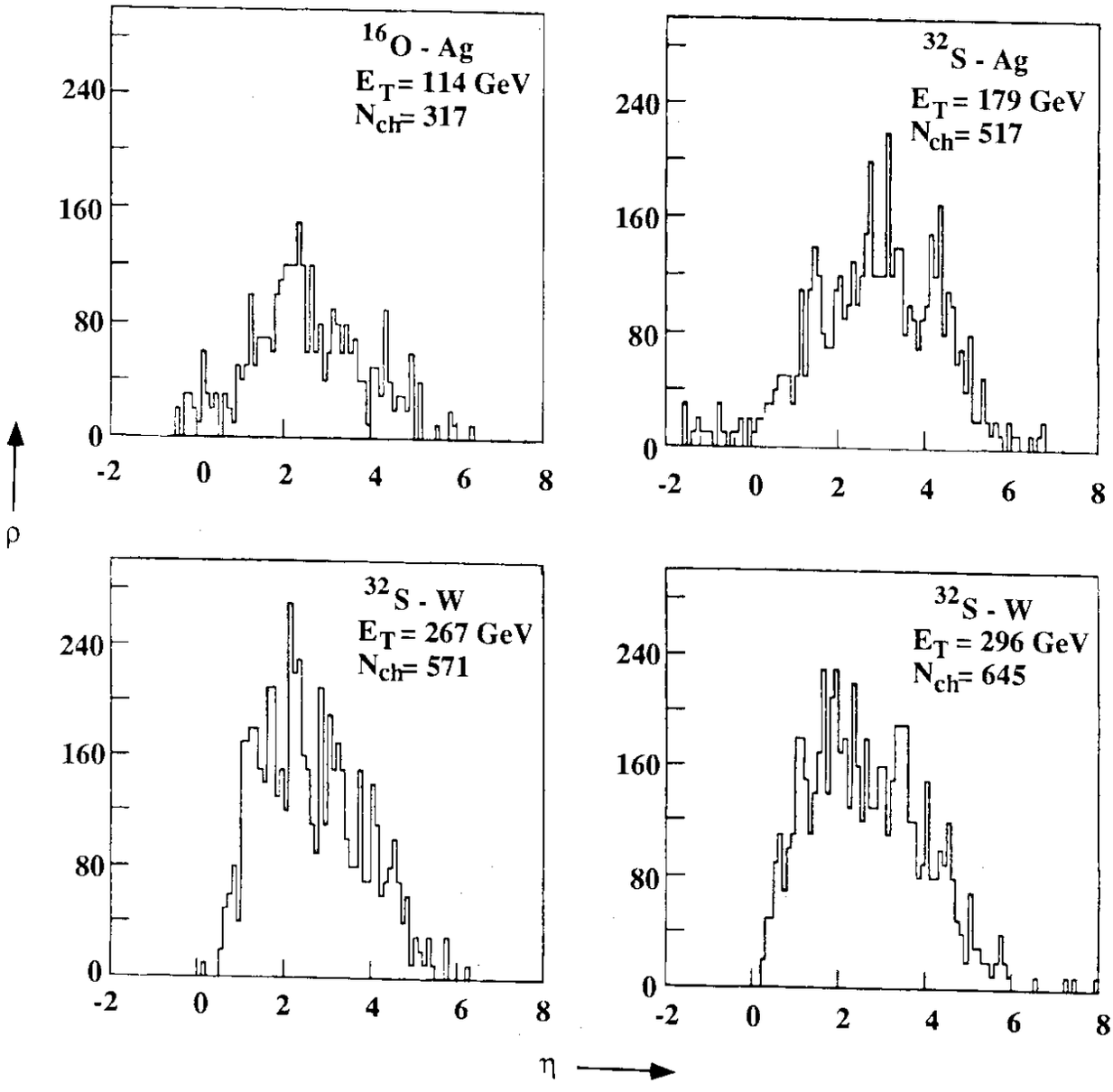
^{16}O - Ag
E_T = 114 GeV
N_{ch} = 317
^{32}S - Ag
E_T = 179 GeV
N_{ch} = 517
^{32}S - W
E_T = 267 GeV
N_{ch} = 571
^{32}S - W
E_T = 296 GeV
N_{ch} = 645
240
160
80
0
-2
0
2
4
6
8
ρ
η

Fig. 8b

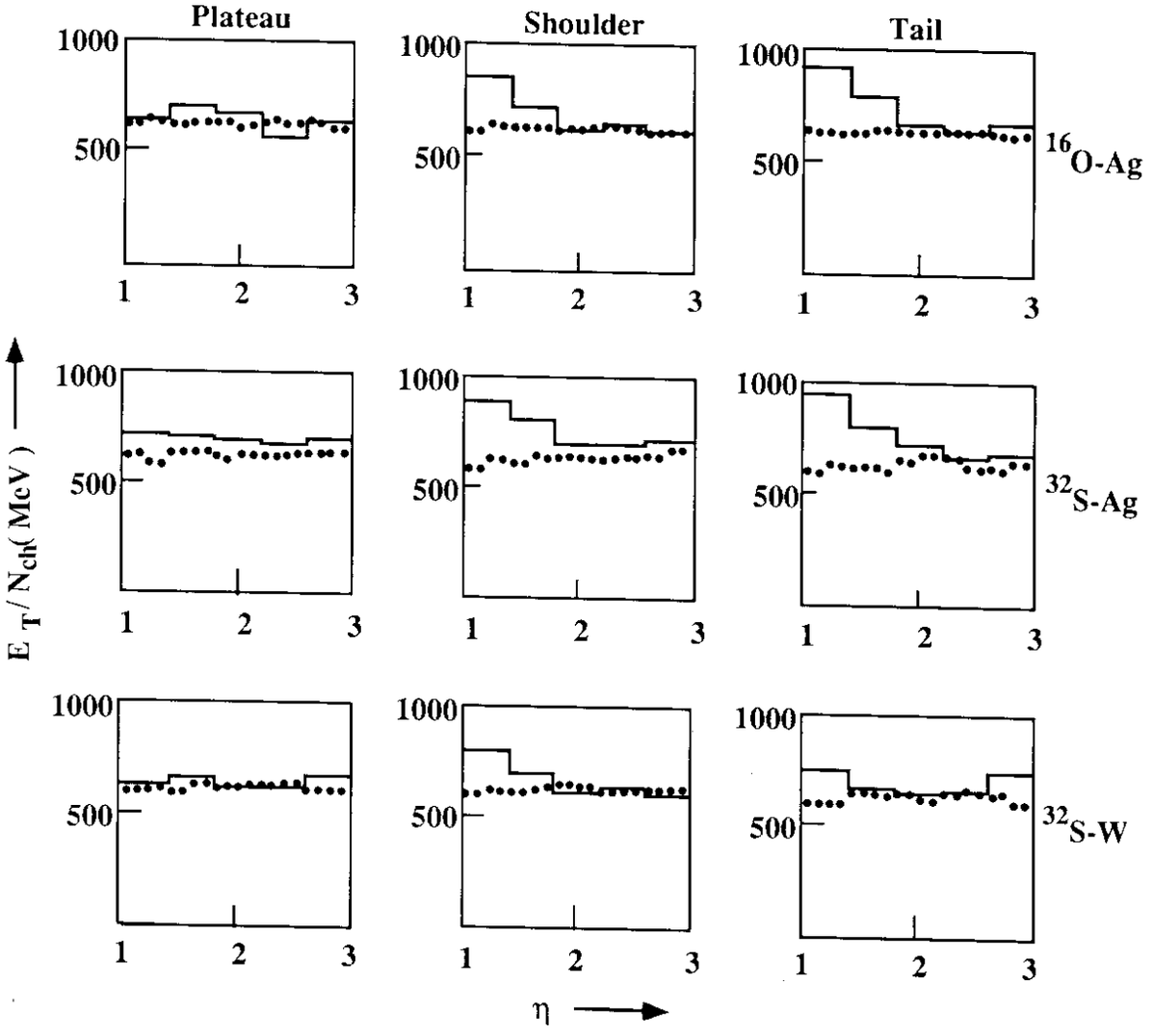
Plateau
Shoulder
Tail
1000
500
1
2
3
^{16}O-Ag
^{32}S-Ag
^{32}S-W
E_T / N_{ch} (MeV)
η

Fig. 9

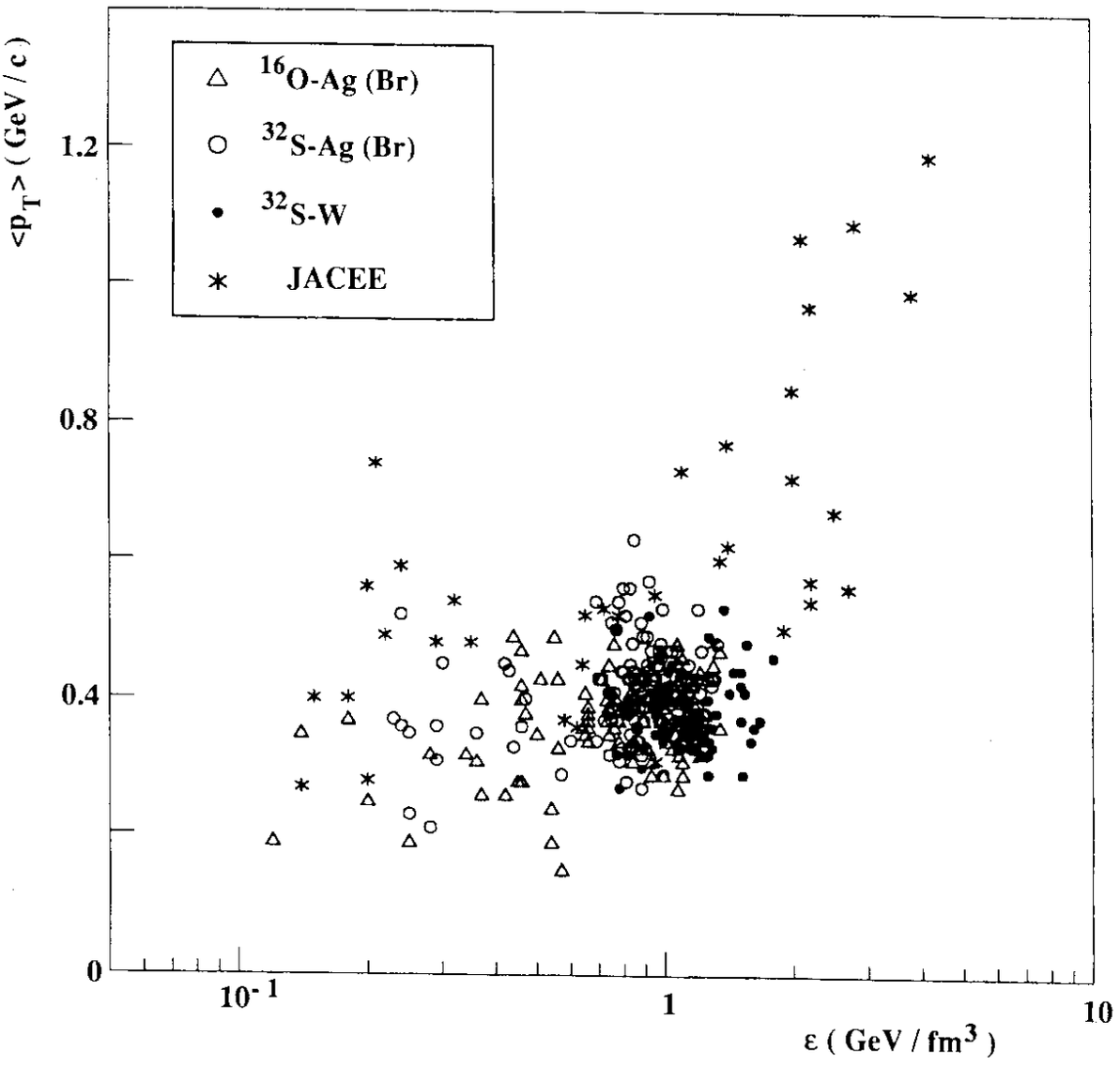

Fig. 10